Society of Medical Education & Research

2022, Volume 2, Issue 1, Page No: 106-121

ISSN: 3108-4834

Archive of International Journal of Cancer and Allied Science

Methylation of cg24067911 Inhibits Colorectal Cancer Metastasis via the BCL6–ATXN1–CDH1 Pathway

Luis Felipe Vargas[1]*, Ricardo Jose Torres[1]

[1]Department of Cancer Research, Pontificia Universidad Católica de Chile, Santiago, Chile.

***E-mail** ✉ l.vargas.puc@gmail.com

Abstract

DNA methylation critically influences colorectal cancer (CRC) development and metastasis, yet the precise effects at individual genomic sites are not fully elucidated. Previously, we found that hypomethylation at cg24067911 correlates with poor outcomes in CRC patients. To clarify the role of cg24067911 in metastatic progression, we used the CRISPR-dCas9-DNMT3a system to selectively modify its methylation. Integrating transposase-accessible chromatin sequencing, RNA sequencing, and chromatin immunoprecipitation revealed that cg24067911 lies within an ATXN1 enhancer and serves as a binding site for BCL6. Reduced methylation at this locus strengthened BCL6 interaction, boosting ATXN1 expression. In turn, ATXN1 functions as a transcriptional regulator of CDH2, driving epithelial-mesenchymal transition and enhancing metastatic potential in CRC. These findings uncover a novel epigenetic pathway—the BCL6–ATXN1–CDH2 axis—through which cg24067911 methylation impacts metastasis, highlight its prognostic value, and propose targeted epigenetic editing as a potential therapeutic approach to limit CRC spread.

Keywords: Methylation, cg24067911, Colorectal cancer, BCL6–ATXN1–CDH1

Introduction

Colorectal cancer (CRC) is the third most frequently diagnosed malignancy worldwide, with both incidence and mortality steadily rising [1]. At the time of diagnosis, roughly 20% of CRC patients already present with metastases, and even among those initially treated with curative intent, about a quarter eventually develop metastatic disease [2]. Improving prognostic predictions and identifying patients at risk of metastasis remains a key focus in CRC research [3, 4]. Because metastatic CRC is linked to poor outcomes and limited therapeutic options, understanding the molecular drivers of metastasis is critical for designing effective interventions. While numerous studies have investigated genetic mutations, metastasis-initiating cells, epithelial-mesenchymal transition (EMT), and the tumor microenvironment [5], these insights have yet to translate into substantial reductions in clinical metastasis rates.

Epigenetic regulation, especially DNA methylation, has emerged as a major factor influencing gene expression and CRC metastatic potential [6]. Methylation-based biomarkers have shown strong utility in both cancer diagnosis and prognosis [7]. Evidence indicates that CRC tumors with and without metastatic spread display distinct methylation landscapes, with many methylation patterns established prior to the onset of metastasis [8], suggesting a contributory role of DNA methylation in facilitating metastatic progression. Traditional studies have largely relied on global methyltransferase inhibitors such as decitabine or azacitidine, limiting the ability to pinpoint locus-specific effects. The advent of CRISPR technology has enabled precise genomic editing, and innovations such as dCas9 fused to DNA methyltransferases or demethylases (e.g., DNMT3A)

Access this article online https://smerpub.com/

Received: 21 January 2022; **Accepted:** 23 April 2022

How to cite this article: Vargas LF, Torres RJ. Methylation of cg24067911 Inhibits Colorectal Cancer Metastasis via the BCL6–ATXN1–CDH1 Pathway. Arch Int J Cancer Allied Sci. 2022;2(1):106-21. https://doi.org/10.51847/QEoZbYMsKw

allow targeted manipulation of methylation at specific CpG sites [9]. This precision facilitates exploration of direct causal relationships between DNA methylation changes and cancer phenotypes and may guide the development of highly specific epigenetic therapies.

In previous work, we generated predictive models for CRC diagnosis and prognosis based on cell-free DNA methylation profiles from a cohort of 801 CRC patients and 1021 controls, achieving high predictive accuracy [10]. Among the identified markers, cg24067911 was notable for its potential both as a diagnostic indicator and as a predictor of metastasis, pointing to a functional role in CRC progression. The CpG site cg24067911 is novel and has not been characterized previously. Its host gene, ATXN1, encodes a protein involved in transcriptional repression and participates in the Notch signaling pathway [11]. While research on ATXN1 has predominantly focused on neurological diseases [12–14], its role in cancer remains largely unexplored.

In this study, we applied CRISPR/dCas9-DNMT3a to selectively edit the methylation status of cg24067911 and investigated its effect on CRC metastasis using both cell-based and animal models. We further explored ATXN1 as a downstream mediator and discovered that it can act as a transcription factor to upregulate CDH2 (N-cadherin), promoting EMT and facilitating metastatic behavior in CRC. Finally, we validated the clinical relevance of the cg24067911/ATXN1 axis, revealing a previously unrecognized epigenetic mechanism underlying CRC metastasis.

Materials and Methods

Ethics statements

Written informed consent was obtained from all patients prior to sample collection. The study protocol received approval from the Medical Ethics Committee of Sun Yat-sen University Cancer Center (approval number B2017-019-01). Animal experiments were conducted following the guidelines of the Animal Ethics Committee of Sun Yat-sen University (approval number L102012021020G).

Human specimens

To assess cg24067911 methylation levels, droplet digital PCR (ddPCR) was performed on 40 tumor–normal tissue pairs from 20 patients. ATXN1 mRNA expression was analyzed using quantitative real-time PCR (qRT-PCR) on 84 paired tumor and adjacent normal tissues from 42 patients. Protein expression of ATXN1 was examined via immunohistochemistry (IHC) in 488 paired formalin-fixed, paraffin-embedded samples derived from 244 patients.

Maintenance of cell lines

Human colorectal cancer (CRC) cell lines such as DLD-1, HCT116, SW480, RKO, and SW620, along with the non-tumorigenic HEK-293T cells, were obtained from the American Type Culture Collection (ATCC) and stored as frozen stocks in the lab. SW480 and SW620 cells were grown in Dulbecco's modified Eagle's medium (DMEM; GIBCO, #C11995500BT), whereas DLD-1 and HCT116 were propagated in RPMI 1640 medium (GIBCO, #C11875500BT). RKO cells were cultured in minimum essential medium (MEM; GIBCO, #C11095500BT) supplemented with non-essential amino acids (GIBCO, #11140050). All media contained 10% fetal bovine serum (FBS; TransGen Biotech, #FS301-02) and 1% penicillin-streptomycin mixture (100 U/mL penicillin and 100 μg/mL streptomycin; BasalMedia, #S110JV). Cells were incubated in a humidified atmosphere with 5% CO_2 at 37 °C. Authentication of cell lines was confirmed recently via short tandem repeat (STR) analysis, and all were verified to be free of mycoplasma contamination.

Animal experiments

HCT116 and SW620 cells were maintained under the conditions outlined above. Female NSG mice aged six weeks (sourced from Bestest100, Zhuhai, China) were placed under anesthesia and received intrasplenic injections of 1.5×10^6 HCT116 or DLD-1 cells per animal. Similarly, six-week-old female Balb/c nude mice (Bestest100, Zhuhai, China) were administered 2.5×10^6 SW620 cells via the portal vein. In vivo imaging was conducted at 2 or 4 weeks following injection. Cells from HCT116 or SW620 lines were subjected to ATXN1 silencing or treated with a negative control (NC). Animal health was monitored regularly, and euthanasia by CO_2 asphyxiation was performed upon reaching endpoints, including end of study, tumor ulceration, ≥20% body weight reduction, or signs of severe distress. Livers were harvested post-euthanasia and subjected to hematoxylin and eosin (H&E) staining.

Construction of plasmids and viral transduction

To knock down specific genes, small interfering RNAs (siRNAs) directed against ATXN1 and BCL6 were

designed and produced by RiboBio (Guangzhou, China). Transfection into cells was achieved using Lipofectamine RNAiMax reagent (Thermo Fisher Scientific, #13778150). For generating stable ATXN1 knockdown or overexpression lines, lentiviral particles were produced in HEK-293T cells using shRNA constructs for ATXN1 knockdown or an ATXN1 overexpression vector. CRC cells were then transduced with these lentiviruses for 18–24 hours with 8 μg/mL polybrene (Beyotime, #C0351), followed by puromycin selection (InvivoGen, #ant-pr-1) at suitable concentrations for a minimum of 7 days.

Site-specific DNA methylation editing

Guide RNAs (sgRNAs) were cloned into the pdCas9-DNMT3a-EGFP plasmid (Addgene; synthesized by Lianfeng, Shanghai, China) or the pPB-dCas9-DNMT3a-EGFP vector (VectorBuilder, Guangzhou, China). CRC cell lines received transfection with the dCas9-DNMT3a-sgRNA construct. For piggyBac-based systems, DLD-1 and HCT116 cells were co-transfected with PB-dCas9-DNMT3a-sgRNA and the hyPBase transposase plasmid. Cells expressing EGFP were isolated by fluorescence-activated cell sorting (FACS). Successful methylation induction at the CpG site cg24067911 in sorted populations was confirmed.

Bisulfite pyrosequencing analysis

Genomic DNA from cultured cells was isolated with the TIANamp Genomic DNA Kit (TIANGEN BIOTECH, #DP304), and concentrations were standardized using a NanoDrop spectrophotometer. Bisulfite modification and cleanup of DNA were carried out with the EpiTect Bisulfite Kit (Qiagen, #59104). Assay-specific primers were developed with PyroMark Assay Design 2.0 software (Qiagen), and amplification was performed using KAPA2G Robust HotStart PCR Kit (ROCHE, #K5525) under these thermal conditions: 95 °C for 3 min initial hold; 40 cycles of 94 °C for 30 s, 56 °C for 30 s, and 72 °C for 1 min; followed by 72 °C for 7 min final extension. PCR products underwent pyrosequencing, and methylation percentages at cg24067911, an adjacent CpG site, and the ATXN1 promoter region were determined quantitatively on the PyroMark Q96 ID system (Qiagen) as described previously [15, 16]. Data processing for methylation at individual sites was handled automatically by Pyro Q-CpG software.

Immunoblotting

Protein extracts from cells or tissues were prepared, and concentrations were quantified via BCA assay (Invivogen, #23227). Equivalent protein loads were resolved by SDS-polyacrylamide gel electrophoresis and blotted onto PVDF membranes. Membranes were blocked in 5% non-fat milk in TBST for ≥1 hour at room temperature, then probed overnight at 4 °C with primary antibodies: anti-ATXN1 (1:1000; Novus Biologicals, #NBP1-51689), anti-β-actin (1:1000; Cell Signaling Technology, #3700), anti-N-cadherin (1:5000; Proteintech, #66219-1-Ig), anti-E-cadherin (1:5000; Proteintech, #60335-1-Ig), and anti-Vimentin (1:20000; Proteintech, #10366-1-AP). After TBST washes, incubation with HRP-linked secondary antibodies occurred for 1 hour at room temperature. Bands were detected using an enhanced chemiluminescence kit (Tanon, #180-5001 A) and captured on a chemiluminescent imager. β-Actin served as the internal loading control.

Real-time quantitative PCR (RT-qPCR)

Total RNA was purified from cells or tissues using the RNA-Quick Purification Kit (ES Science, #RN001), followed by cDNA synthesis with PrimeScript™ RT Master Mix (Takara, #RR036Q). Reactions for qPCR were assembled with cDNA, gene-specific primers, and master mix (Promega, #A6001), then run on a LightCycler 480 system (Roche) per the supplier's guidelines. Experiments on cells were done in triplicate. Gene expression levels relative to controls were calculated using the $2^{-\Delta\Delta Ct}$ method.

Cell migration assay using transwell chambers

Inserts with 8 μm pores (Corning, #353097) were inserted into 24-well plates. Cells deprived of serum for 24 hours were plated at 2–2.5 × 10^5 cells per upper chamber. The bottom chamber contained medium with 20% FBS as chemoattractant. Following 24 hours incubation, cells remaining on the top side were wiped off, while those that had migrated to the bottom were fixed in 4% paraformaldehyde, stained with 0.1% crystal violet, and imaged. Migrated cells were enumerated in five randomly selected fields per insert under microscopy, with counts normalized relative to the control condition.

Matrigel-based invasion assay

Transwell chambers featuring 8 μm pores were pre-coated with Matrigel (diluted 1:10 in serum-free

medium; 60 µL per insert), inserted into 24-well plates (Corning, #353097), and allowed to solidify at 37°C for 1 hour. Following 24 hours of serum deprivation, 5×10^5 cells were placed into each upper compartment. The bottom compartment contained medium supplemented with 20% FBS as a chemoattractant. After a 24-hour incubation period, cells that failed to invade were wiped from the top surface, while those that had traversed to the underside were fixed using 4% paraformaldehyde and stained with 0.1% crystal violet solution. Invaded cells were then enumerated in randomly selected fields per insert via microscopy, with counts quantified and expressed relative to the control condition.

Wound healing migration assay

Before plating cells into 6-well dishes at a density sufficient to achieve confluence the next day, reference lines were drawn on the underside of each well. The following day, uniform scratches were carefully made across the monolayer using sterile 200 µL pipette tips, oriented perpendicular to the pre-marked lines. Old medium was removed, wells were rinsed with PBS to eliminate detached debris, and fresh medium was added for continued incubation. Photographs of the scratch regions were taken using a Leica X microscope (Leica, Germany) immediately after wounding (as time zero) and subsequently at 24-hour intervals. Wound closure was quantified by measuring areas with ImageJ software, and migration rates were determined by comparing changes in wound width across time points and experimental groups.

Cell proliferation assay (MTT)

Cells were inoculated into 96-well plates at 5000 cells per well and cultured for designated durations (24, 48, 72, 96, and 120 hours). At each specified time point, MTT reagent (Beyotime, #C0009S) was introduced to the relevant wells and incubated for 4 hours. Resulting formazan crystals were solubilized in DMSO, and optical density was recorded at 490 nm on a plate reader. Proliferation rates were expressed as percentages of absorbance values relative to the control group. All assays were conducted in triplicate.

Chromatin immunoprecipitation (ChIP)

ChIP experiments were performed with the MAGnify Chromatin Immunoprecipitation System (Invitrogen, #492024), adhering to the provided protocol. Sheared chromatin was pulled down using antibodies against ATXN1 (1:100; Novus Biologicals, #NBP1-51689), BCL6 (1:200; Cell Signaling Technology, #5650), or IgG as a negative control (Cell Signaling Technology, #3900). Enrichment of potential transcription factor binding to target cis-regulatory elements was assessed by PCR, with results expressed as percentage of input DNA. Amplicons were resolved by agarose gel electrophoresis. Primer details are provided in the Supplementary Materials.

Dual-luciferase reporter assay

Cells were co-transfected with a firefly luciferase reporter construct harboring the cis-regulatory sequence (Synbio Technologies) and the pRL-TK Renilla luciferase vector for normalization. Luciferase activities were measured using the Dual-Luciferase Reporter Assay System (Promega, #E1910) following the manufacturer's guidelines. Data were normalized by computing the ratio of firefly to Renilla luciferase signals.

Droplet digital PCR (ddPCR)

Genomic DNA from cells or tissues was isolated with the TIANamp Genomic DNA Kit (TIANGEN, #DP304) and subjected to bisulfite conversion via the EZ DNA Methylation-Lightning™ Kit (ZYMO RESEARCH, #D5031). Reaction mixtures comprising bisulfite-treated DNA, gene-specific primers and probes, ddPCR Supermix (BIO-RAD, #1863024), and Droplet Generation Oil (BIO-RAD, #1863005) were loaded into DG8 Cartridges (BIO-RAD, #1864008) for emulsion generation. Droplets underwent amplification on a T100 Thermal Cycler, followed by readout on the QX200™ Droplet Reader. All procedures followed manufacturer instructions, with cellular experiments performed in triplicate. Methylation at cg24067911 was quantified using QuantaSoft™ Analysis Pro software.

Immunohistochemical (IHC) staining

IHC was carried out on paraffin-embedded samples as described previously [17]. Stained slides were evaluated and scored blindly by two independent pathologists, yielding a composite score. IHC scores were contrasted between cancerous and adjacent non-cancerous tissues. For expression stratification, the threshold distinguishing high versus low ATXN1 levels was set at 91.25 (range: 0–160) based on ROC curve analysis of tumor tissue IHC scores in each cohort.

Statistical methods

Comparisons employed Student's t-test or Chi-square test as appropriate. Results are presented as mean ± standard deviation (SD) and were processed using SPSS 21.0 or GraphPad Prism 9.3 software. Statistical significance was defined as $P < 0.05$. Kaplan-Meier curves were generated for survival analysis, with differences assessed via Log-Rank test.

Results and Discussion

Characterization of cg24067911's involvement in CRC metastasis

Previous work from our group established hypomethylation at cg24067911 as a marker for diagnosis and prognosis in colorectal cancer (CRC) **(Figures 1a and 1b)**. In both our patient cohort [10] and TCGA datasets, methylation at this site was markedly lower in tumor tissues relative to normal mucosa **(Figure 1a)**. Validation by droplet digital PCR in matched samples further showed escalating hypomethylation with disease progression, as metastatic sites displayed substantially reduced methylation compared to primary tumors. Moreover, patients experiencing recurrence or distant metastasis post-resection exhibited more severe hypomethylation than those without relapse. Together, these findings highlight a strong link between cg24067911 hypomethylation and increased tumor aggressiveness.

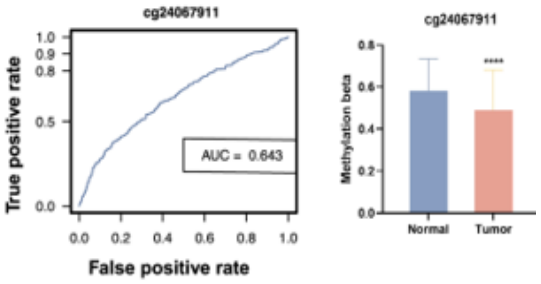

a)

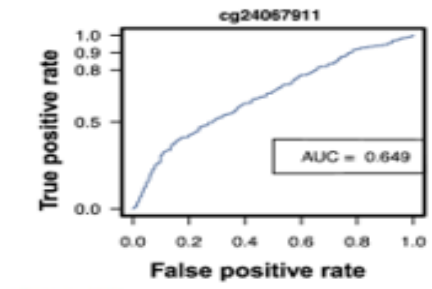

b)

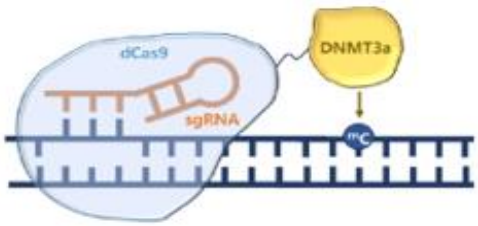

c)

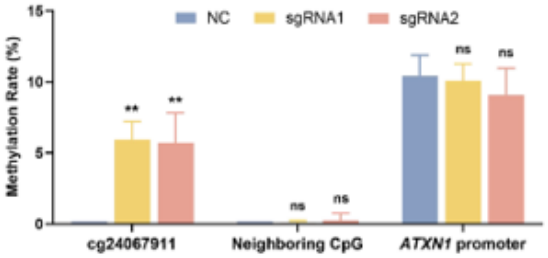

d)

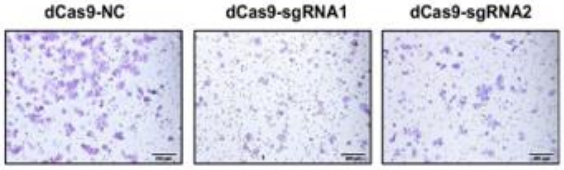

e)

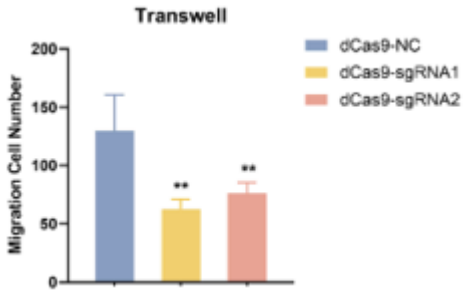

f)

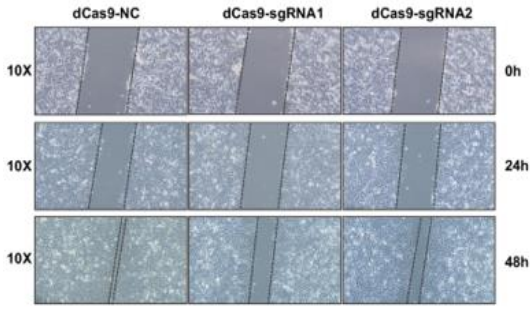

g)

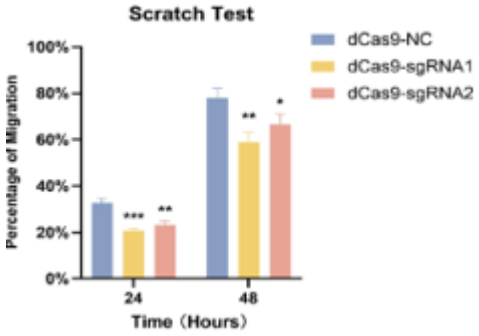

h)

Figure 1. Methylation Status at cg24067911 Impacts Migration and Metastasis in Colorectal Cancer (CRC)

a Reduced methylation at cg24067911 serves as a diagnostic indicator for CRC. Left panel displays the receiver operating characteristic (ROC) curve evaluating cg24067911 as a marker for CRC detection using data from patients at Sun Yat-sen University Cancer Center (previously described). Right panel shows a box plot comparing methylation levels in cell-free DNA from normal individuals and CRC cases at the same center (Tumor: n=801; Normal: n=1021). AUC denotes area under the curve.

b Lower methylation at cg24067911 acts as a marker for CRC prognosis and correlates with unfavorable outcomes, based on prior patient data from Sun Yat-sen University Cancer Center. Upper panel presents the ROC curve for prognostic utility of cg24067911. Lower panel illustrates the link between cg24067911 hypomethylation and reduced survival. AUC, area under curve; HR, hazard ratio; CI, confidence interval.

c Diagram illustrating the CRISPR-dCas9-DNMT3a system for site-specific DNA methylation editing. DNMT3a refers to DNA (Cytosine-5-)-Methyltransferase 3 Alpha.

d Pyrosequencing assessment of methylation percentages at cg24067911, an adjacent CpG locus, and the ATXN1 promoter region in cells treated with dCas9-DNMT3a versus controls. Analyzed by Student's t-test.

e Example micrographs from Transwell migration experiments using dCas9-DNMT3a-modified DLD-1 cells compared to controls.

f Quantification of migrated cells in Transwell assays for dCas9-DNMT3a-treated versus control DLD-1 cells. Student's t-test applied.

g Representative micrographs of wound healing assays in dCas9-DNMT3a-modified DLD-1 cells versus controls.

H Quantitative analysis of wound closure rates in scratch assays for dCas9-DNMT3a-treated versus control DLD-1 cells. Student's t-test used. Results expressed as mean ± SD; significance levels: *P < 0.05, **P < 0.01, ***P < 0.001; ns, not significant.

To determine if reduced methylation at cg24067911 directly contributes to CRC advancement, a CRISPR-dCas9-DNMT3a-based approach was applied to elevate methylation specifically at this CpG site **(Figure 1c)**. Functional assays were then performed in vitro to assess related malignant traits in CRC models. Successful site-directed hypermethylation was achieved at cg24067911 in DLD-1 human colorectal carcinoma cells, as confirmed by pyrosequencing. Methylation markedly rose at the intended locus (noted as cg24067911), with no notable alterations at the closest flanking CpG or within the ATXN1 promoter **(Figure 1d)**. A piggyBac transposon-based delivery of the dCas9-DNMT3a construct in CRC lines was also employed, with validation via ddPCR and pyrosequencing yielding comparable outcomes to the initial lentiviral method. Cells with induced hypermethylation via dCas9-DNMT3a exhibited diminished migratory capacity in both Transwell **(Figures 1e and 1f)** and wound healing experiments **(Figures 1g and 1h)**. In contrast, MTT proliferation assays revealed no appreciable differences in growth rates between hypermethylated and control cells. Collectively, these functional studies in vitro indicate that hypomethylation at cg24067911 promotes migratory behavior in CRC cells, whereas forced methylation at this site attenuates metastatic potential.

Characterization of cg24067911 as an enhancer element regulating ATXN1 transcription

The cg24067911 site resides in the 5' untranslated region (UTR) of ATXN1 **(Figure 2a)**, raising the potential for methylation changes to affect expression of this gene. Transcriptomic profiling via RNA sequencing indicated reduced ATXN1 mRNA in dCas9-DNMT3a-treated cells relative to controls, a finding corroborated by RT-qPCR **(Figures 2b and 2c)**. Given DNA methylation's role in epigenetic control, the regulatory landscape around cg24067911 was interrogated further. Public databases, including the UCSC Genome Browser and WashU Epigenome Browser, were queried for histone mark

ChIP-seq datasets at this locus. Enrichment of H3K4me1 and H3K27ac signals was observed around cg24067911 in CRC cells, consistent with an active enhancer. Notably, stronger H3K27ac accumulation in CRC versus normal colonic epithelium suggested enhancer activation specific to malignancy **(Figure 2d)**. As methylation is known to restrict chromatin accessibility and transcription factor recruitment at regulatory elements, ATAC-seq was conducted, revealing reduced openness at the cg24067911-containing region in hypermethylated DLD-1 cells compared to controls **(Figure 2e)**. These observations support the notion that methylation status at cg24067911 modulates enhancer activity.

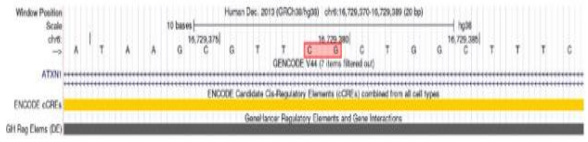

a)

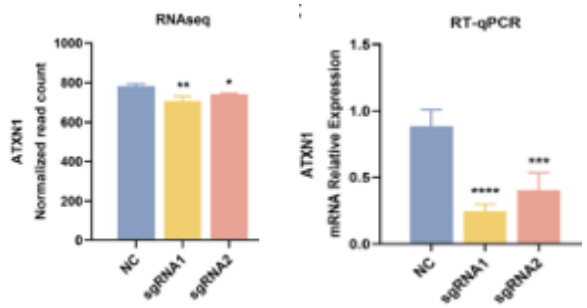

b) c)

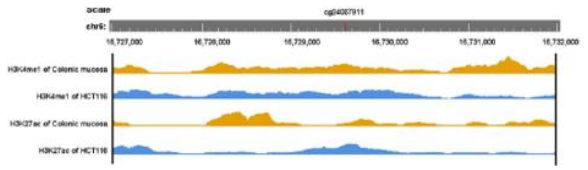

d)

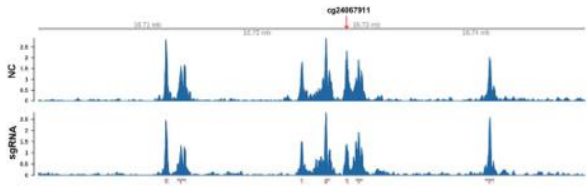

e)

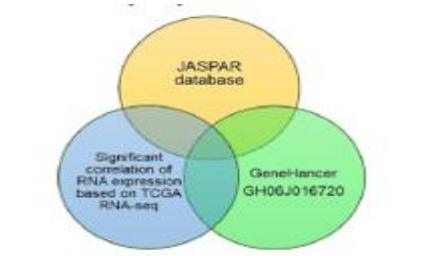

Genes	Correlation	P for correlation
BCL6	0.6939	<0.001
FOSL2	0.3555	<0.001
MZF1	0.1680	<0.001
JUND	-0.1143	0.0047

f)

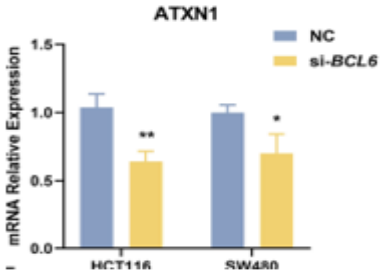

g)

h)

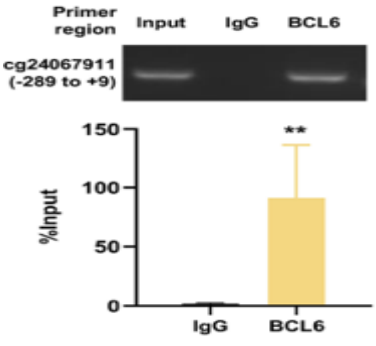

i)

Figure 2. Methylation at cg24067911 affects the Functional Activity of the Resident Enhancer **a** Screenshot from the UCSC Genome Browser displaying the position of cg24067911 in relation to nearby regulatory elements.

b Normalized RNA-seq read counts for ATXN1 in dCas9-DNMT3a-modified cells compared with control cells.
c RT-qPCR confirmation of ATXN1 transcript levels in dCas9-DNMT3a-treated cells versus controls. Statistical analysis by Student's t-test.
d ChIP-seq tracks for histone marks H3K4me1 and H3K27ac in normal colon tissue and the HCT116 colorectal cancer cell line, obtained from the WashU Epigenome Browser. The red arrow points to cg24067911.
e ATAC-seq profiles demonstrating lower chromatin accessibility at the cg24067911 locus in dCas9-DNMT3a-treated cells relative to controls. Red arrow highlights the cg24067911 position.
f Upper section: Venn diagram outlining the strategy for selecting candidate transcription factors (TFs) that may bind near cg24067911. Lower section: Summary of expression correlations between ATXN1 and the leading candidate TFs (JUND, FOSL2, MZF1, BCL6).
g RT-qPCR measurement of ATXN1 mRNA levels following BCL6 knockdown in CRC cell lines compared to controls.
h Consensus DNA-binding motif predicted for BCL6.
i Chromatin immunoprecipitation (ChIP) evidence for BCL6 recruitment to the enhancer containing cg24067911. Upper panel: Agarose gel image of PCR products from ChIP-enriched DNA showing BCL6 binding to the target enhancer sequence. Lower panel: Quantitative PCR results of ChIP enrichment. Analyzed with Student's t-test. Values are mean ± SD; *P < 0.05, **P < 0.01, ***P < 0.001.

Further efforts were directed toward pinpointing the transcription factor responsible for enhancer-mediated regulation. Potential binding TFs for the cg24067911 region were identified through queries in the JASPAR (https://jaspar.elixir.no/) database and GeneHancer resource [18]. Candidates were refined by identifying those whose expression significantly correlated with ATXN1 mRNA levels in the TCGA colorectal cancer dataset **(Figure 2f)**. Transient knockdown of the four strongest candidates using siRNAs (si-BCL6, si-FOSL2, si-MZF1, si-JUND) revealed that only BCL6 depletion substantially reduced ATXN1 expression **(Figure 2g)**. Direct binding of BCL6 to the enhancer harboring cg24067911 was confirmed via ChIP experiments **(Figures 2h and 2i)**. Additionally, treatment of BCL6-knockdown CRC cells with the global demethylating agent decitabine or the TET inhibitor bobcat339 consistently lowered ATXN1 levels across conditions, suggesting that broad-spectrum epigenetic modulators have minimal specific impact on this regulatory axis.

ATXN1 drives metastatic behavior in CRC

The precise contribution of ATXN1 to colorectal cancer biology, particularly as a potential effector downstream of cg24067911 methylation, required clarification. Accordingly, ATXN1 was either silenced or ectopically expressed in multiple CRC cell lines. Functional migration assays, including Transwell and wound healing experiments, showed that reduced ATXN1 expression markedly suppressed cell motility, whereas forced ATXN1 overexpression enhanced metastatic traits **(Figures 3a–3d)**. However, MTT-based proliferation assessments indicated no notable impact of altered ATXN1 levels on cell growth. Furthermore, ATXN1 was overexpressed in DLD-1 and HCT116 cells already carrying the dCas9-sgRNA3 hypermethylation system. Subsequent Matrigel invasion and scratch wound healing assays revealed restoration of migratory and invasive capabilities in these cells **(Figures 3e and 3f)**.

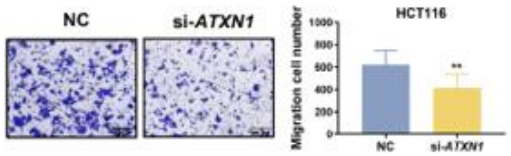

a)

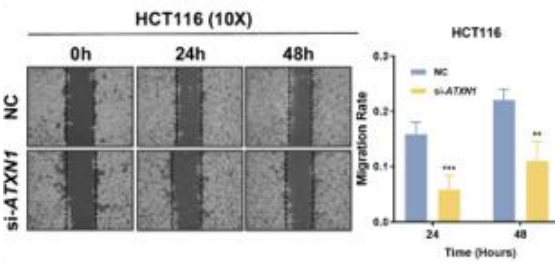

b)

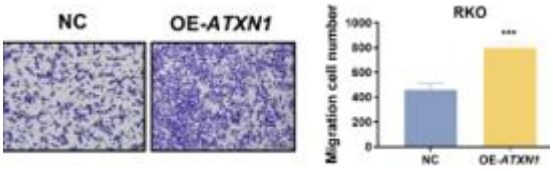

c)

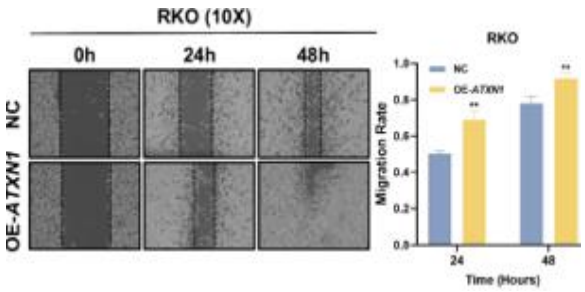

d)

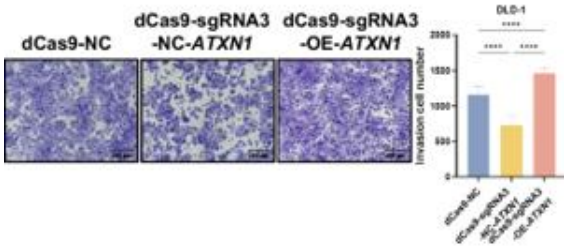

e)

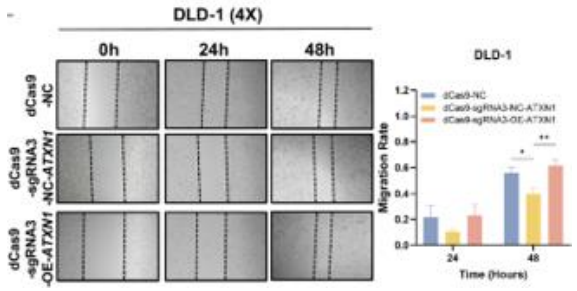

f)

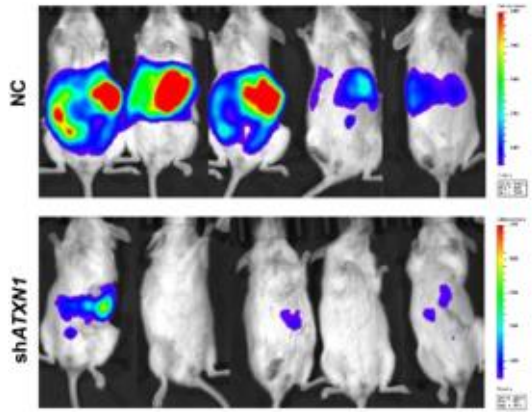

g)

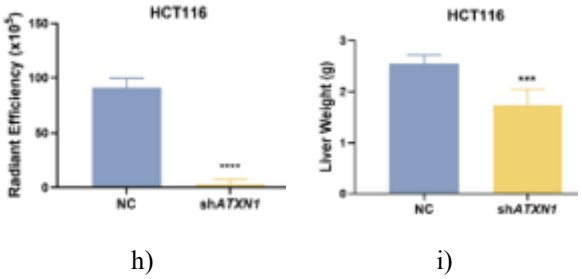

h) i)

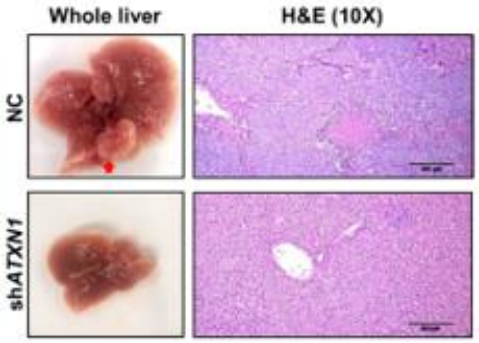

j)

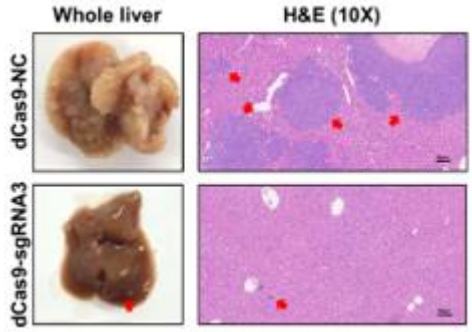

k)

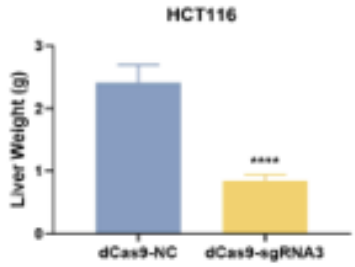

l)

Figure 3. ATXN1 promotes metastasis in colorectal cancer both in vitro and in vivo

a Left: Example micrographs; right: quantification of Transwell migration assays in HCT116 cells with ATXN1 knockdown compared to negative control (NC). Analyzed by Student's t-test.

b Left: Representative images; right: quantitative data from scratch wound healing assays in HCT116 cells subjected to ATXN1 knockdown versus NC. Student's t-test.
c Left: Example micrographs; right: quantification of Transwell migration assays in RKO cells overexpressing ATXN1 relative to controls. Student's t-test.
d Left: Representative images; right: quantitative analysis of wound healing assays in RKO cells with ATXN1 overexpression compared to controls. Student's t-test.
e Left: Example micrographs; right: quantification of Matrigel invasion assays in DLD-1 cells. Student's t-test.
f Left: Representative images; right: quantitative data from scratch wound healing assays in DLD-1 cells. Student's t-test.
g–h In vivo bioluminescence imaging (g) of liver metastases in NSG mice following intrasplenic injection of HCT116 cells with ATXN1 knockdown or NC, accompanied by a bar graph (h) showing radiant efficiency of metastatic signals. Student's t-test.
i, j Bar graph of liver weights (i) and representative macroscopic and H&E-stained microscopic images (j) of livers from NSG mice injected intrasplenically with ATXN1-knockdown or control HCT116 cells. Student's t-test.
k, l Representative macroscopic and microscopic images (k) along with a bar graph of liver weights (l) from NSG mice receiving intrasplenic injection of HCT116 cells with ATXN1 knockdown versus NC. Student's t-test.
Data are presented as mean ± SD; *P < 0.05, **P < 0.01, ***P < 0.001.

The role of ATXN1 in CRC was additionally confirmed in vivo, where mice injected with shRNA-mediated ATXN1-knockdown cells developed markedly fewer liver metastatic nodules compared to those receiving control cells **(Figures 3g–3j)**. Moreover, liver metastasis models established using dCas9-sgRNA3 cells (with elevated cg24067911 methylation) and corresponding controls revealed that increasing methylation at this site substantially suppressed metastatic spread **(Figures 3k and 3l)**. These observations aligned with the effects of cg24067911 methylation status, suggesting that this CpG site exerts its influence on CRC metastasis, at least in part, through downstream regulation of ATXN1.

ATXN1 regulates epithelial-mesenchymal transition (EMT) by controlling CDH2 expression as a transcription factor

The mechanistic interplay likely involves both cg24067911 methylation and ATXN1 expression levels. To explore affected pathways, GO and KEGG enrichment analyses were performed on differentially expressed genes associated with cg24067911 hypermethylation and low ATXN1 expression in the COAD cohort from TCGA. Pathways related to cell adhesion emerged as commonly enriched under both conditions **(Figure 4a)**. Gene set enrichment analysis (GSEA) further identified significant involvement of the EMT pathway in ATXN1-related signatures **(Figure 4b)**, providing a potential explanation for how the cg24067911/ATXN1 axis drives CRC metastasis. Subsequent experiments assessed ATXN1's impact on EMT markers. Western blotting and RT-qPCR showed that ATXN1 depletion reduced CDH2 (N-cadherin) levels while elevating CDH1 (E-cadherin) expression **(Figures 4c and 4d)**. These changes were reversed upon ATXN1 overexpression **(Figures 4c and 4e)**. Protein-protein interaction networks, queried via the STRING (https://cn.string-db.org/), database, revealed a direct association between ATXN1 and CDH2 among EMT-related genes **(Figure 4f)**. These findings indicate that CDH2 may serve as a critical downstream mediator through which the cg24067911/ATXN1 regulatory module promotes metastatic behavior in CRC.

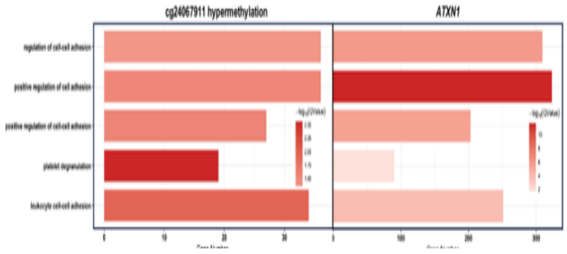

a)

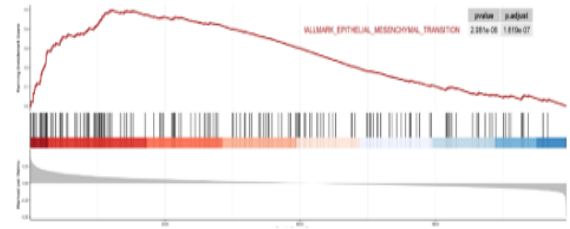

b)

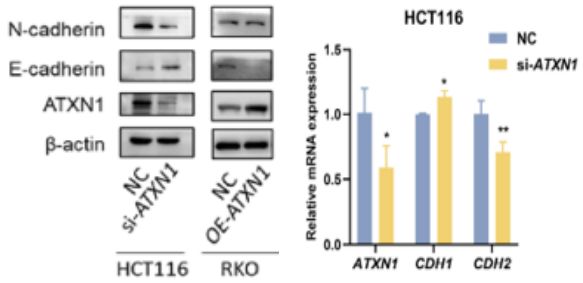

c) d)

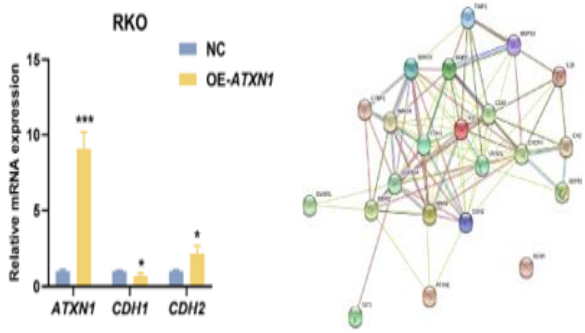

e) f)

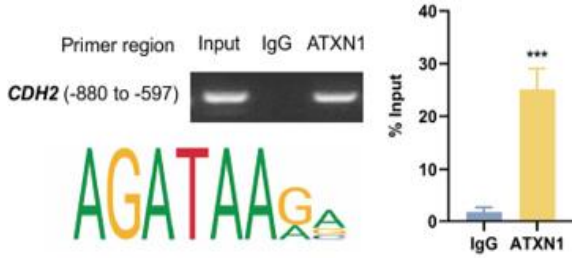

g)

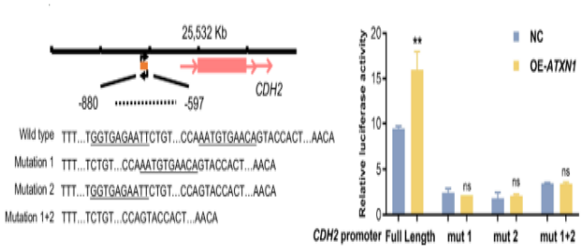

h)

Figure 4. ATXN1 Drives Epithelial-Mesenchymal Transition (EMT) by Serving as a Transcription Factor for CDH2 (N-cadherin)

a GO/KEGG pathway enrichment analysis linked to cg24067911 methylation and ATXN1 expression. Left panel: Box plot displaying shared GO terms enriched among differentially expressed genes (DEGs) in hypermethylated cg24067911 conditions (dCas9-DNMT3a-treated DLD-1 cells versus controls). Right panel: Box plot of shared GO terms enriched among DEGs associated with low versus high ATXN1 expression. GO, Gene Ontology.

b Gene set enrichment analysis (GSEA) plot showing ATXN1-related signatures enriched in the Hallmark EMT pathway.

c Western blot analysis of ATXN1 and EMT markers (E-cadherin and N-cadherin) in HCT116 cells with siRNA-mediated ATXN1 knockdown and in RKO cells overexpressing ATXN1.

d, e RT-qPCR quantification of ATXN1, CDH1, and CDH2 transcripts in ATXN1-knockdown HCT116 cells (D) and ATXN1-overexpressing RKO cells (E). Analyzed by Student's t-test.

f Network visualization of protein-protein interactions between ATXN1 and EMT-related genes.

g Evaluation of ATXN1 binding to the CDH2 promoter. Upper left: Agarose gel electrophoresis of ChIP-PCR products. Lower left: Predicted ATXN1 binding motif. Right: Quantitative PCR results from ChIP-enriched DNA.

h Dual-luciferase reporter assay assessing ATXN1-mediated transcriptional activation of the CDH2 promoter. Left: Schematic of the wild-type CDH2 promoter construct and designed mutations. Right: Relative luciferase activity measurements comparing wild-type and mutated promoters in cells with ATXN1 overexpression versus controls. Student's t-test.

Data are presented as mean ± SD; *P < 0.05, **P < 0.01, ***P < 0.001.

Given prior reports that ATXN1 functions as a transcription factor capable of binding DNA or chromatin [11], we performed ATXN1-specific ChIP assays and confirmed direct binding to the CDH2 promoter region (TSS -880 to -597) **(Figure 4g)**. Dual-luciferase reporter assays further revealed that ATXN1 occupancy significantly boosted CDH2 promoter activity, an effect that was abolished upon mutation of the binding sites **(Figure 4h)**. Collectively, these results elucidate the mechanistic cascade: hypomethylation at cg24067911 elevates ATXN1 expression, enabling ATXN1 to act as a transcriptional activator of CDH2, thereby increasing N-cadherin levels and ultimately facilitating CRC metastasis.

Clinical relevance of ATXN1 in colorectal cancer specimens

ATXN1 transcript levels were measured by RT-qPCR in retrospectively acquired CRC tissues and matched adjacent normal mucosa, revealing markedly higher expression in tumors **(Figure 5a)**. Consistent upregulation in CRC versus normal samples was also evident from publicly available datasets in the Oncomine database **(Figures 5b and 5c)**. Immunohistochemical analysis similarly demonstrated stronger ATXN1 protein staining in tumor sections compared to normal tissue **(Figure 5d)**. Correlation with clinicopathological features showed that elevated ATXN1 was particularly associated with stage IV disease, oxaliplatin resistance, and recurrence **(Figures 5e–5g)**. Prognostically, patients exhibiting high ATXN1 levels experienced significantly reduced overall survival (OS) relative to those with low expression **(Figure 5h)**, as well as shorter disease-free survival (DFS) among stage III cases **(Figure 5i)**. Survival analysis of the TCGA COAD cohort corroborated these findings, linking higher ATXN1 expression to poorer DFS **(Figure 5j)**.

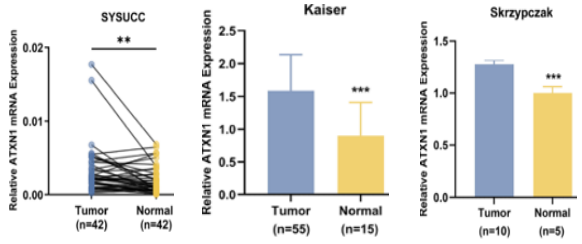

a) b) c)

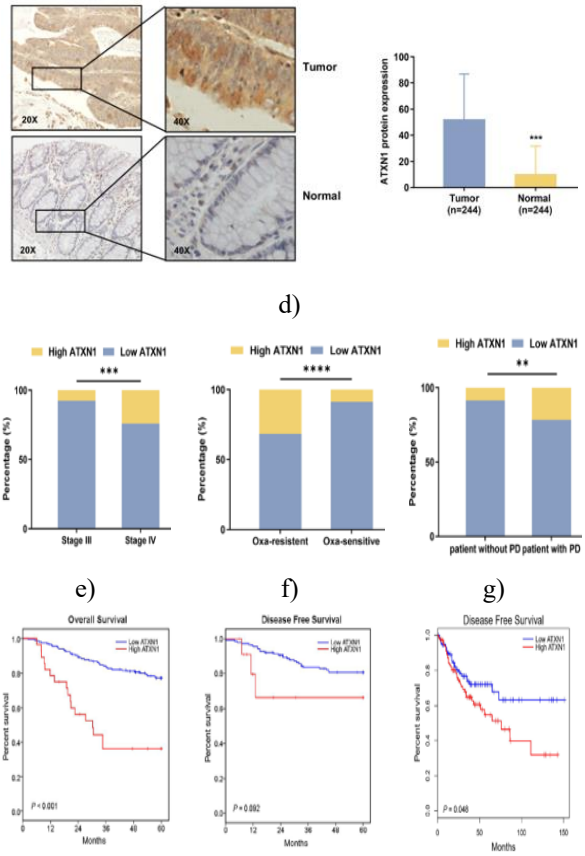

d) e) f) g) h) i) j)

Figure 5. Clinical Association of ATXN1 with Metastasis and Prognosis in Colorectal Cancer

a RT-qPCR quantification of ATXN1 mRNA in matched tumor and adjacent normal tissues retrospectively obtained from Sun Yat-sen University Cancer Center. Analyzed by paired Student's t-test.

b, c Relative ATXN1 transcript levels in CRC tumors versus normal colon tissues, derived from Oncomine datasets curated by Kaiser (B) and Skrzypczak (C).

d Immunohistochemical (IHC) assessment of ATXN1 protein in CRC versus paired normal mucosa. Left: Representative micrographs of ATXN1-stained tumor and adjacent normal samples. Right: Box plot summarizing IHC scores for ATXN1. Student's t-test.

e Box plot comparing ATXN1 expression in stage III versus stage IV CRC patients from SYSUCC. Chi-square test.

f Box plot of ATXN1 levels in oxaliplatin-sensitive versus oxaliplatin-resistant patients from SYSUCC. Chi-square test.

g Box plot displaying ATXN1 expression in stage III patients with or without disease progression from SYSUCC. Chi-square test.
h Kaplan-Meier overall survival (OS) curves for CRC patients stratified by ATXN1 expression levels from SYSUCC. Log-Rank test.
i Kaplan-Meier disease-free survival (DFS) curves for stage III CRC patients grouped by ATXN1 expression from SYSUCC. Log-Rank test.
j Kaplan-Meier DFS curves for patients in the TCGA CRC cohort stratified according to ATXN1 expression. Log-Rank test.
Data are presented as mean ± SD; *P < 0.05, **P < 0.01, ***P < 0.001.

Despite progress in CRC screening and therapeutic strategies, enhancing diagnostic accuracy and treatment efficacy remains essential. DNA methylation represents a key epigenetic hallmark in CRC research. Colorectal tumors commonly exhibit genome-wide hypomethylation alongside promoter-specific hypermethylation relative to healthy colonic tissue [19]. Such dysregulation can silence tumor suppressors or activate oncogenes, driving proliferation and malignant transformation. These patterns underpin the CpG island methylator phenotype (CIMP) classification, dividing patients into CIMP-high and CIMP-low subtypes with distinct prognostic implications [20, 21]. Several individual methylated loci have been proposed as predictors of prognosis or metastasis, including MPPED2 [22], SOX4 [23], and genes such as FIGN, HTRA3, BDNF, HCN4, and STAC2 [24], though mechanistic insights are often limited. Deeper investigations into regulatory mechanisms are rarer, with examples like SLIT1 and ANGPTL4 in CRC metastasis [25, 26] relying on small cohorts for target identification. The current work builds on large-scale clinical screening that identified cg24067911 as a robust diagnostic and metastasis-associated marker in CRC [9].

DNA demethylating agents, including 5-azacytidine and decitabine, are established in hematologic malignancies [27]. Emerging epigenetic therapies have demonstrated potential against CRC in preclinical models and early-phase trials [28], reversing aberrant methylation to restore suppressor function and synergize with standard chemotherapy [29]. However, their non-specific action limits utility in solid tumors. Recent advances in CRISPR-based epigenetic editing offer greater precision. The original CRISPR/Cas9 system combines guide RNA with nuclease-active Cas9 for genome cleavage [30]. Catalytically dead Cas9 (dCas9) retains DNA targeting via sgRNA but lacks cutting activity [9]. Fusion with effectors like DNMT3a or Tet1 enables site-directed methylation or demethylation. When paired with locus-specific sgRNA, these dCas9-effector complexes provide versatile tools for precise epigenetic modulation and potential targeted therapy. CRISPR/dCas9-DNMT3a has efficiently altered methylation and gene expression at selected sites. For instance, it corrected hypomethylation at the amyloid precursor protein (APP) promoter in Alzheimer's models, lowering APP and Aβ levels [31]. In vivo lentiviral delivery similarly induced APP hypermethylation in mouse brain, improving behavioral outcomes and supporting therapeutic applicability. In oncology, the approach has successfully addressed cancer-relevant epigenetic marks [32–35]. Here, cg24067911 was mapped to an ATXN1 enhancer. Application of CRISPR/dCas9-DNMT3a revealed that targeted hypermethylation at this site suppresses CRC invasion via downregulation of ATXN1.

While our site-specific methylation editing yielded substantial effects, partial efficiency aligns with reports on challenges in enhancer targeting. Incomplete methylation may arise from restricted chromatin access, as BCL6 occupancy maintains openness, potentially resisting DNMT3a recruitment. Interactions with histone modifiers, such as EZH2-generated H3K27me3 facilitating DNMT activity, could preserve epigenetic state. Prior work has linked ATXN1 to EMT regulation in a Notch-dependent fashion [11, 36]. EMT is central to metastatic dissemination [37, 38]. A defining feature, "cadherin switching"—downregulation of E-cadherin and upregulation of N-cadherin—marks progression to mesenchymal traits [39]. N-cadherin, typical of mesenchymal cells, promotes loss of epithelial polarity and invasive behavior [40]. Its elevation correlates with advanced malignancy and poorer outcomes [41, 42]. Although N-cadherin's role in EMT and metastasis is established, upstream epigenetic control remains underexplored. This study demonstrates that hypermethylation at cg24067911 reduces ATXN1 expression, where ATXN1 directly transactivates CDH2, elevating N-cadherin to drive EMT, diminish cell adhesion, and enhance CRC metastasis. Recurrent cg24067911 hypomethylation likely involves multifactorial processes: early field cancerization demethylates premalignant tissue, priming for oncogenesis, while disrupted BCL6-ATXN1 signaling

reinforces hypomethylation via a positive feedback loop sustaining BCL6 binding **(Figure 2)**. Clinically, this offers opportunities for non-invasive detection via serial liquid biopsy and therapeutic targeting, potentially with EZH2 inhibitors to exploit BCL6 reliance.

Conclusion

This investigation leverages extensive cohort data alongside comprehensive in vitro and in vivo validation to delineate cg24067911's mechanistic impact. Results show that cg24067911 hypomethylation facilitates BCL6 recruitment, boosting ATXN1 expression and thereby accelerating EMT. Additional research is warranted to assess translational potential of CRISPR/dCas9-DNMT3a targeting cg24067911 in CRC management.

Acknowledgments: None

Conflict of Interest: None

Financial Support: None

Ethics Statement: None

References

1. Morgan E, Arnold M, Gini A, Lorenzoni V, Cabasag CJ, Laversanne M, et al. Global burden of colorectal cancer in 2020 and 2040: incidence and mortality estimates from GLOBOCAN. Gut. 2023;72:338–44.
2. Biller LH, Schrag D. Diagnosis and treatment of metastatic colorectal cancer: a review. JAMA. 2021;325:669–85.
3. Zhao J, Jiang O, Chen X, Liu Q, Li X, Wu M, et al. Development and validation of a prediction model for metastasis in colorectal cancer based on LncRNA CRNDE and radiomics. 2022. 1:e6.
4. Zhang Q, Xu Y, Kang S, Chen J, Yao Z, Wang H et al. A novel computational framework for integrating multidimensional data to enhance accuracy in predicting the prognosis of colorectal cancer. 2022. 1:e27.
5. Shin AE, Giancotti FG, Rustgi AK. Metastatic colorectal cancer: mechanisms and emerging therapeutics. Trends Pharm Sci. 2023;44:222–36.
6. Su R, Wu X, Tao L, Wang C. The role of epigenetic modifications in Colorectal Cancer Metastasis. Clin Exp Metastasis. 2022;39:521–39.
7. Koch A, Joosten SC, Feng Z, de Ruijter TC, Draht MX, Melotte V, et al. Analysis of DNA methylation in cancer: location revisited. Nat Rev Clin Oncol. 2018;15:459–66.
8. Ju HX, An B, Okamoto Y, Shinjo K, Kanemitsu Y, Komori K, et al. Distinct profiles of epigenetic evolution between colorectal cancers with and without metastasis. Am J Pathol. 2011;178:1835–46.
9. Rahman MM, Tollefsbol TO. Targeting cancer epigenetics with CRISPR-dCAS9: Principles and prospects. Methods. 2021;187:77–91.
10. Luo H, Zhao Q, Wei W, Zheng L, Yi S, Li G, et al. Circulating tumor DNA methylation profiles enable early diagnosis, prognosis prediction, and screening for colorectal cancer. Sci Transl Med. 2020;12:eaax7533.
11. Tong X, Gui H, Jin F, Heck BW, Lin P, Ma J, et al. Ataxin-1 and Brother of ataxin-1 are components of the Notch signalling pathway. EMBO Rep. 2011;12:428–35.
12. Ju H, Kokubu H, Lim J. Beyond the glutamine expansion: influence of posttranslational modifications of ataxin-1 in the pathogenesis of spinocerebellar ataxia type 1. Mol Neurobiol. 2014;50:866–74.
13. Xie M, Swanson MS. UTteR control through miRs: fine-tuning ATXN1 levels to prevent ataxia. Genes Dev. 2020;34:1107–9.
14. Suh J, Romano DM, Nitschke L, Herrick SP, DiMarzio BA, Dzhala V, et al. Loss of Ataxin-1 Potentiates Alzheimer's Pathogenesis by Elevating Cerebral BACE1 Transcription. Cell. 2019;178:1159–45.e17.
15. Tost J, Gut IG. DNA methylation analysis by pyrosequencing. Nat Protoc. 2007;2:2265–75.
16. Taylor KH, Kramer RS, Davis JW, Guo J, Duff DJ, Xu D, et al. Ultradeep bisulfite sequencing analysis of DNA methylation patterns in multiple gene promoters by 454 sequencing. Cancer Res. 2007;67:8511–8.
17. Ju HQ, Lu YX, Chen DL, Tian T, Mo HY, Wei XL, et al. Redox Regulation of Stem-like Cells Though the CD44v-xCT Axis in Colorectal Cancer: Mechanisms and Therapeutic Implications. Theranostics. 2016;6:1160–75.
18. Fishilevich S, Nudel R, Rappaport N, Hadar R, Plaschkes I, Iny Stein T, et al. GeneHancer: genome-wide integration of enhancers and target genes in GeneCards. Database (Oxford). 2017;2017:bax028.

19. Bian S, Hou Y, Zhou X, Li X, Yong J, Wang Y, et al. Single-cell multiomics sequencing and analyses of human colorectal cancer. Science. 2018;362:1060–3.
20. Walther A, Johnstone E, Swanton C, Midgley R, Tomlinson I, Kerr D. Genetic prognostic and predictive markers in colorectal cancer. Nat Rev Cancer. 2009;9:489–99.
21. Schweiger MR, Hussong M, Röhr C, Lehrach H. Genomics and epigenomics of colorectal cancer. Wiley Interdiscip Rev Syst Biol Med. 2013;5:205–19.
22. Gu S, Lin S, Ye D, Qian S, Jiang D, Zhang X, et al. Genome-wide methylation profiling identified novel differentially hypermethylated biomarker MPPED2 in colorectal cancer. Clin Epigenet. 2019;11:41.
23. Rezayi Soufiani A, Dolatkhah R, Raeisi M, Chavoshi H, Mohammadi P, Mehdinavaz Aghdam A. Hypermethylation of MIR129-2 Regulates SOX4 Transcription and Associates with Metastasis in Patients with Colorectal Cancer. J Gastrointest Cancer. 2022;53:718–24.
24. Ili C, Buchegger K, Demond H, Castillo-Fernandez J, Kelsey G, Zanella L, et al. Landscape of genome-Wide DNA methylation of colorectal cancer metastasis. Cancers (Basel). 2020;12:2710.
25. Zhang K, Zhai Z, Yu S, Tao Y. DNA methylation mediated down-regulation of ANGPTL4 promotes colorectal cancer metastasis by activating the ERK pathway. J Cancer. 2021;12:5473–85.
26. Shuai W, Wu J, Chen S, Liu R, Ye Z, Kuang C, et al. SUV39H2 promotes colorectal cancer proliferation and metastasis via tri-methylation of the SLIT1 promoter. Cancer Lett. 2018;422:56–69.
27. Pappalardi MB, Keenan K, Cockerill M, Kellner WA, Stowell A, Sherk C, et al. Discovery of a first-in-class reversible DNMT1-selective inhibitor with improved tolerability and efficacy in acute myeloid leukemia. Nat Cancer. 2021;2:1002–17.
28. Rezapour S, Hosseinzadeh E, Marofi F, Hassanzadeh A. Epigenetic-based therapy for colorectal cancer: Prospect and involved mechanisms. J Cell Physiol. 2019;234:19366–83. Article CAS PubMed Google Scholar
29. Peng PL, Qin SY, Lei L, He ZJ, Li BW, Edouard N, et al. Epigenetic remodeling under oxidative stress: mechanisms driving tumor metastasis. MedComm – Oncol. 2024;3:e70000.
30. Wang SW, Gao C, Zheng YM, Yi L, Lu JC, Huang XY, et al. Current applications and future perspective of CRISPR/Cas9 gene editing in cancer. Mol Cancer. 2022;21:57.
31. Park H, Shin J, Kim Y, Saito T, Saido TC, Kim J. CRISPR/dCas9-Dnmt3a-mediated targeted DNA methylation of APP rescues brain pathology in a mouse model of Alzheimer's disease. Transl Neurodegener. 2022;11:41.
32. Wang H, Guo R, Du Z, Bai L, Li L, Cui J, et al. Epigenetic Targeting of Granulin in Hepatoma Cells by Synthetic CRISPR dCas9 Epi-suppressors. Mol Ther Nucleic Acids. 2018;11:23–33.
33. Sarno F, Goubert D, Logie E, Rutten MGS, Koncz M, Deben C, et al. Functional Validation of the Putative Oncogenic Activity of PLAU. Biomedicines. 2022;11:102.
34. Lu H, Zhang Q, He S, Liu S, Xie Z, Li X, et al. Reduction-Sensitive Fluorinated-Pt(IV) Universal Transfection Nanoplatform Facilitating CT45-Targeted CRISPR/dCas9 Activation for Synergistic and Individualized Treatment of Ovarian Cancer. Small. 2021;17:e2102494.
35. Elumalai P, Ezhilarasan D, Lakshmi T. Targeting head and neck cancer epigenetics with CRISPR-dCas9: An emerging therapeutic approach. Oral Oncol. 2022;127:105801.
36. Kang AR, An HT, Ko J, Kang S. Ataxin-1 regulates epithelial-mesenchymal transition of cervical cancer cells. Oncotarget. 2017;8:18248–59.
37. Khan SU, Fatima K, Malik F, Kalkavan H, Wani A. Cancer metastasis: Molecular mechanisms and clinical perspectives. Pharm Ther. 2023;250:108522.
38. Tao L, Zhou Y, Qiu JH, Xiao YZ, Zou J, Zhang Y, et al. Epigenetic regulation in cancer therapy: from mechanisms to clinical advances. MedComm – Oncol. 2024;3:e59.
39. Nakajima S, Doi R, Toyoda E, Tsuji S, Wada M, Koizumi M, et al. N-cadherin expression and epithelial-mesenchymal transition in pancreatic carcinoma. Clin Cancer Res. 2004;10:4125–33.
40. Serrano-Gomez SJ, Maziveyi M, Alahari SK. Regulation of epithelial-mesenchymal transition through epigenetic and post-translational modifications. Mol Cancer. 2016;15:18.
41. Ye Z, Zhou M, Tian B, Wu B, Li J. Expression of lncRNA-CCAT1, E-cadherin and N-cadherin in

colorectal cancer and its clinical significance. Int J Clin Exp Med. 2015;8:3707–15.

42. Yan X, Yan L, Liu S, Shan Z, Tian Y, Jin Z. N-cadherin, a novel prognostic biomarker, drives malignant progression of colorectal cancer. Mol Med Rep. 2015;12:2999–3006.